

This document is the Accepted Manuscript version of a Published Work that appeared in final form in ACS Applied Materials & Interfaces, copyright © American Chemical Society after peer review and technical editing by the publisher. To access the final edited and published work see <https://doi.org/10.1021/acsami.7b05186>.

Bifunctional Electrocatalysts for Oxygen Reduction and Borohydride Oxidation Reactions Using Ag₃Sn Nano-Intermetallic on Ensemble Effect

Qiao Wang,[†] Fuyi Chen,^{*,†} Yaxing Liu,[†] Nan Zhang,[†] Liang An[&] and Roy L. Johnston^{*,‡}

[†] State Key Laboratory of Solidification Processing, Northwestern Polytechnical University, Xian, 710072, China

[&] Department of Mechanical Engineering, The Hong Kong Polytechnic University, Hung Hom, Kowloon, Hong Kong SAR, China

[‡] Department of Chemistry, University of Birmingham, Birmingham, B15 2TT, UK

KEYWORDS: oxophilic metal, intermetallic Ag₃Sn, oxygen reduction reaction, borohydride oxidation reaction, ensemble effect

Abstract: Incorporating an oxophilic metal into the noble metal to produce a cost-effective Ag₃Sn nano-intermetallic is an emerging approach to enhance the catalytic activity of monometallic Ag in fuel cells, which is different from previous notions that consider a transition metal to increase the catalytic property of Pt. The Ag₃Sn electrocatalyst is prepared by a facile electrodeposition method and exhibits high catalytic performance for the oxygen reduction reaction (ORR) and borohydride oxidation reaction (BOR). The Ag₃Sn electrocatalyst has a ORR specific activity of 0.246 mA cm⁻², 1.3 times greater than the value of the commercial Pt/C (0.187 mA cm⁻²) and a long-term stability with 11 mV decrement in the half-wave potential and 7.01% loss of the diffusion limiting current density after 2000 cycles, superior to Pt/C. Moreover, the Ag₃Sn electrocatalyst delivers a surprisingly higher BOR current density of 11.332 mA cm⁻² than most of bimetallic Ag alloys. The better ORR catalytic activities of Ag-based alloys may arise from the ensemble effect, in which Sn atoms may promote the oxygen adsorption and Ag atoms may contribute to remove the reaction products.

INTRODUCTION

Highly efficient and clean fuel cells have long been considered a promising method to solve the environmental and energy problems raised by the extensive use of fossil fuels.¹⁻³ Liquid fuel cells, fed with borohydride⁴, methanol^{5, 6}, ethanol^{7, 8}, or formic acid⁹, can efficiently transform chemical energy of fuels into electricity with low pollution. Among these liquid fuel cells, direct borohydride fuel cell (DBFC) is a rapidly emerging technology due to large hydrogen content (10.6 wt%), high specific energy (9296 Wh/kg) and ease of fuel storage and delivery.¹⁰⁻¹³ However, a critical barrier to the development and commercialization of DBFC is lack of highly active and stable electrocatalyst for O₂ reduction at cathode and NaBH₄ oxidation at anode.

Platinum (Pt) and its alloys have been proven as the state-of-the-art bifunctional electrocatalysts in the DBFC.¹⁴⁻¹⁷ Nevertheless, the unfavorable catalytic activity towards hydrolysis side reaction (i.e., $\text{NaBH}_4 + 2\text{H}_2\text{O} \rightarrow \text{NaBO}_2 + 4\text{H}_2$) lowers the faradic efficiency, accompanied the safety and cost problem.¹⁸ Extensive efforts have been committed to replace Pt-based electrocatalysts using effective, economical, and earth-abundant bifunctional electrocatalysts. Among them, Ag has been a major focus of research and development, owing to acceptable catalytic activity, superior stability in alkaline electrolytes and the significant cost (0.7 \$/g) advantage over Pt (40 \$/g).^{19, 20} In particular, Ag has little catalytic activity for hydrolysis side reaction.²¹ However, the oxygen reduction reaction (ORR) at pure silver commonly suffers from higher overpotentials (200 mV) than the commercial Pt/C. The primary approaches to modify the catalytic performance of Ag monometallic catalysts have been on the bimetallic catalysts by nanoalloys. As an example of crystallographically disordered alloy, the carbon-supported AgNi core-shell nanocatalyst²² (Ni@Ag/C) exhibited a superior borohydride oxidation reaction (BOR) activity than Ag/C. The DBFC with Ni₁@Ag₁/C electrocatalysts obtained the

maximum power density of 8.54 mW cm^{-2} . Silver copper core-shell electrocatalyst supported on carbon (Cu@Ag/C)²³ showed an enhanced BOR activity and the power density reached 17.27 mW cm^{-2} using $\text{Cu}_2\text{@Ag}_1\text{/C}$ as anode catalyst. Duan et al. investigated the carbon-supported AgCu (AgCu/C) nanoparticles with different atomic ratios and found that the $\text{Ag}_{33}\text{Cu}_{67}\text{/C}$ electrocatalyst showed better BOR activity.²⁴ Adam et al. reported the carbon-supported AgCo alloy nanoparticles had a high and stable ORR activity.²⁵

Bimetallic catalysts are the effective approaches to improve the catalytic activity of Ag monometallic catalysts. AgNi, AgCu and AgCo have considerably improved the catalytic performance, however, they suffer from low alloying due to the transition metals (such as Co, Ni, Cu) chosen to alloy with Ag. Generally, Ag is highly miscible with only two other transition or noble metals, that is Au and Pd.²⁶ However, alloying with the two noble metals introduces the new problem of high cost. To form Ag-based alloys with the inexpensive but immiscible transition metals (Co, Ni, Cu) where Ag preferentially exhibits surface segregation, the two currently used methods are the rapid quenching method (such as Ag-Cu metallic glasses with high solubility obtained via pulsed laser deposition)²⁷ and the precursor reduction method (for example via formation of Ag-Co bimetallic precursors)²⁵. However, the rapid quenching method is technologically difficult and expensive for large-scale production. In addition, the precursor reduction method often requires extreme conditions (harmful chemicals, high temperature or complicated experimental procedures) at the sacrifice of time.

Some main group metals (such as Mg, Ba, Bi, Sn) possess high solubility in Ag-based ordered intermetallic phases, and inducing crystallographic order has been shown to improve the activity of certain electrocatalysts.²⁸⁻³¹ For example, the $\text{Ag}_4\text{Sn}^{31}$ intermetallic electrocatalyst displays enhanced ORR electrocatalytic activity and good methanol-tolerant property in alkaline

media, however, use of some main group metals (e.g. Mg and Ba) have been limited by their easy dissolution in alkaline media, the phase pure Ag-Sn intermetallics have not been investigated for their BOR activities.

The enhanced catalytic performance of bimetallic catalysts may be attributed to the electronic, geometric, and/or ensemble effects.^{9, 32} In general, electronic effects (electron transfer among different metals) and geometric effects (compressive or tensile strain), affect the bonding with reactants, intermediates and products.⁹ Ensemble effects, different metals in the surface complement catalyzing distinct reaction steps, have been observed for nanoalloys (e.g. PtSn, PdSn, PdAu, AgPd) in gas-phase heterogeneous catalysis and electrocatalysis.^{14, 33-35}

In this work, we design a new strategy of incorporating an oxophilic Sn metal into the inexpensive Ag metal to produce a new Ag₃Sn intermetallic with higher catalytic property. The nano-intermetallic Ag₃Sn catalyst was synthesized by a facile electrodeposition approach without any surfactants for the first time. The as-synthesized Ag₃Sn intermetallic compound exhibited good catalytic activity towards ORR and BOR coupled with improved durability in alkaline media compared with pure Ag catalyst. The mechanism for the enhanced ORR performance in Ag₃Sn catalysts is closely related to the strong oxygen affinities of Sn element and the weak oxygen affinities of Ag element. Such an approach, combining bimetallic elements with strong and weak oxygen affinities as in an intermetallic compounds, may open up a novel way to gain efficient and stable Ag-based electrocatalyst for both ORR and BOR application.

RESULTS AND DISCUSSION

Structural Characterization of Ag-Sn electrocatalyst

The XRD patterns of pure Ag and Ag₃Sn catalysts deposited on Cu substrate are shown in Figure 1a. The four diffraction peaks at 37.60°, 39.49°, 51.91°, and 69.0° can be seen, corresponding to the (002), (111), (112), and (113) planes of orthorhombic Ag₃Sn phase (JCPDS card No. 04-0800). The XRD peaks of the control sample of pure Ag are in good agreement with face-centered cubic Ag (JCPDS card No. 04-0783). For both samples, two sharp diffraction peaks at 43.30° and 50.43° are assigned to the (111) and (200) planes of Cu substrate (JCPDS card No. 04-0836). The SEM-EDX of the Ag₃Sn catalyst in Figure 1b confirms that the catalyst contains Ag and Sn elements. Figure 1c clearly shows that the Ag₃Sn catalyst has the plate-like morphologies and Figure 1d reveals that the nanoparticles have size of 30 nm in thickness. The SEM images and EDX analysis of Ag_xSn_{100-x} electrocatalysts at different synthesis conditions are presented in Figure S2 and S3. A HRTEM image and the FFT pattern (Figure 1e) indicate that the surface of Ag₃Sn catalyst is enclosed by (111) and (002) planes, based on the lattice fringes. According to the SAED pattern (in Figure 1f), the Ag₃Sn catalyst shows the typical polycrystalline structure with diffraction rings of (111), (002), (200), (112) and (113) facets that belong to the orthorhombic phase Ag₃Sn. It is clear that the crystalline Ag₃Sn catalysts exposed the (111) and (002) facets acting as surface plane with a two-dimensional shape of 30 nm thickness.

Catalytic activity of Ag₃Sn towards the ORR

The ORR activity of pure Ag, Ag₃Sn and Pt/C catalysts was firstly characterized by CV curves in the 0.1 M KOH solution with N₂ or O₂ saturated. As shown in Figure 2a, the Ag₃Sn catalyst exhibited a prominent reduction peak at 0.772 V in the O₂-saturated KOH electrolyte, more positive than pure Ag (0.699 V). As for the commercial Pt/C, a clear reduction peak occurred at 0.855 V. On the contrast, the CV curves of these three catalysts were featureless in

the N₂-saturated electrolyte. For both catalysts, with raising the square roots of scan rates ($v^{1/2}$), the peak currents linearly go up, shown in Figure S4a. This indicates the ORR is controlled by the diffusion process. As displayed in Figure S4b, the specific capacitance of Ag₃Sn at 20 mV s⁻¹ is 1.722 F g⁻¹, a bit bigger than pure Ag (1.412 F g⁻¹). This is due to large specific surface area (electric double layer capacitance) and redox of Ag (pseudocapacitance).³⁶

To further evaluate the O₂ reduction activity of the catalysts, the polarization curves were obtained in oxygen-saturated solution at 1600 rpm (Figure 2b). The half-wave potential ($E_{1/2}$) increased in the order: Pure Ag (0.617 V) < Ag₃Sn (0.772 V) < Pt/C (0.860 V). Pure Sn exhibited less active than pure Ag. For the Ag₃Sn catalyst, the diffusion-limiting current density was comparable to Pt/C. These outcomes suggest Ag-Sn alloy can significantly improve reaction kinetics for the ORR at lower overpotential. Furthermore, the ORR curves of Ag_xSn_{100-x} electrocatalysts at different synthesis conditions are presented in Figure S5. The diffusion-limiting current density, $E_{1/2}$ and E_{onset} summaries of these catalysts are shown in Table S1. The Tafel plots of the catalysts were compared to further analyze the ORR behavior and mechanism in Figure 2c. The Tafel slope of pure Ag was 116.93 mV dec⁻¹, which was within the reported range of 80 to 120 mV dec⁻¹ for Ag-based catalysts³⁶. It was higher than that of Pt/C (77.17 mV dec⁻¹), showing slower O₂ reduction dynamics of pure Ag than Pt. The Tafel slope of the Ag₃Sn catalyst was 92.27 mV dec⁻¹, significantly smaller than pure Ag. The exchange current densities (j_0) were 1.55×10^{-7} A cm⁻², 1.47×10^{-8} and 5.17×10^{-8} for pure Ag, Ag₃Sn, and Pt/C, respectively. The electrochemical active surface area (ECSA) of the commercial Pt/C was estimated by integrating the charge related to hydrogen adsorption (shown in Figure 2d), based on 210 μ C cm⁻² for the adsorption charge of a hydrogen monolayer.³⁷ Figure 2e displays the CVs of Pb UPD on pure Ag and Ag₃Sn catalysts. The adsorption/desorption peak pairs indicated the

formation/dissolution of the metal Pb³⁸. Assuming that the used charge density for a Pb monolayer was 260 $\mu\text{C cm}^{-2}$, the ECSAs of pure Ag and Ag₃Sn catalysts were 0.27 and 0.84 $\text{m}^2 \text{g}^{-1}$, respectively. The ECSAs of pure Ag and Ag₃Sn catalysts were also evaluated by CVs in a N₂-saturated basic solution (Figure S6). The ECSAs of pure Ag and Ag₃Sn catalysts were 0.27 and 0.84 $\text{m}^2 \text{g}^{-1}$, which were calculated using the theoretical value of 400 $\mu\text{C cm}^{-2}$ for Ag oxide³⁸. This coincided with the results calculated from Pb UPD. The Ag₃Sn catalyst had a specific activity (SA) of 0.246 mA cm^{-2} , which was 1.3 times greater than Pt/C (0.187 mA cm^{-2}), and 12 times greater than pure Ag (0.021 mA cm^{-2}), as Figure 2f shows.

It is commonly believed that the O₂ electroreduction catalyzed by Ag-based catalysts in alkaline electrolytes can proceed via two pathways: the two-electron pathway to produce H₂O₂, and the four-electron pathway to produce OH⁻^{14, 39-41}. To understand the O₂ reduction reaction pathway, the polarization curves were performed at rotating rates ranging from 400 to 2500 rpm at a sweep rate of 10 mV s^{-1} and the Koutecky-Levich (K-L) plots obtained from the corresponding ORR data were drawn (Figure 3). The diffusion-limiting current density increases prominently when the rotation rate rises, and the linearity in the K-L plots indicates first-order reaction kinetics towards dissolved oxygen^{37, 42}. The electron transfer number (n) for Ag₃Sn catalyst was approximately 3.70, whereas the n for commercial Pt/C was approximately 4.0, suggesting that Ag₃Sn favors a four-electron reduction process. The n for pure Ag is close to 2, indicating a formation of OOH⁻ as an ORR intermediate. For the Ag_xSn_{100-x} catalysts with varying precursor composition and deposition current, a series of polarization curves and the corresponding K-L plots at different potentials are seen in Figure S7.

The electron transfer number for pure Ag and Ag₃Sn catalysts was about 1.8 and 3.7, obtained from Figure 3. According to the Koutecky-Levich equation (2), the diffusion-limiting

current density is determined by the electron transfer number (n) etc., and the limiting current density for pure Ag and Ag₃Sn was 2.6 and 4.9 mA cm⁻², respectively. So it is established that pure Ag with a lower limiting current value is due to the lower electron transfer number.

In addition to high electrocatalytic activity, high durability is also required for an excellent catalyst in practical applications. The stability was assessed by repeating potential from 0.55 to 1.0 V at 50 mV s⁻¹ in O₂-saturated electrolyte. As displayed in Figure 4, the E_{1/2} of the Ag₃Sn catalyst was negatively shifted about 11 mV, while the E_{1/2} of the commercial Pt/C negatively shifted about 29 mV after 2000 potential cycles. Moreover, the SA of the Ag₃Sn catalyst after the stability test was 0.230 mA cm⁻² with a loss of 22.13% in the ECSA. In contrast, the SA of Pt/C was 0.107 mA cm⁻² and the ECSA reduced by 9.03% from the initial state. The aggregation and dissolution of Pt particles and carbon corrosion with long-term operation make performance loss⁴³. An insight into the structural and morphological evolution of the Ag₃Sn catalyst after potential cycles was obtained by the TEM image, as shown in Figure S8, the original structure and morphology retained well. Therefore, the structure stability of the intermetallic compound may be responsible for the higher durability of the Ag₃Sn catalyst.

Electrocatalytic performance of Ag₃Sn towards the BOR

In view of the effect of OH⁻ on NaBH₄ electrooxidation ($\text{BH}_4^- + 8\text{OH}^- \rightarrow \text{BO}_2^- + 6\text{H}_2\text{O} + 8\text{e}^-$), the CVs for the Ag₃Sn catalyst were recorded in a solution of 5mM NaBH₄ with different NaOH concentration X (X = 0.1, 1, 2 M NaOH), the result is presented in Figure S9a. The oxidation peak current densities increase first from 2.504 to 2.974, and then decrease to 2.563 with increasing X from 0.1 to 2 M. Moreover, as seen from Figure S10, the number of electrons involved for the Ag₃Sn catalyst in X (X = 0.1, 1, 2) M NaOH are derived to be 3.92, 7.64 and

3.53 at 1.1 V, respectively. This is possibly because the electrolyte conductivity increases with adding more NaOH, rendering enhanced catalytic performance; However, excessive OH⁻ tend to compete with BH₄⁻ to adsorb on the catalyst surface, and thereby lower the oxidation current. Therefore, we choose 1M NaOH as the base electrolyte for further study.

Figure S9b shows the BOR activity of the Ag₃Sn catalyst at different NaBH₄ concentrations in 1M NaOH solution. The oxidation peak can be observed, resulting from NaBH₄ electrooxidation. The oxidation peak current densities greatly increased from 1.533 to 11.332 mA cm⁻² as the NaBH₄ concentration increased from 2.5 to 20 mM. Nevertheless, with increasing NaBH₄ concentrations, the oxidation potential shifts more positive. A linear relationship (the peak current density vs NaBH₄ concentration, as in the inset) demonstrates diffusion control during the reaction. Expectedly, for higher NaBH₄ concentrations, the greater overpotential is required to achieve the diffusion control. Therefore, we choose 5 mM NaBH₄ as the main electrolyte for further research.

To compare the electrochemical BOR behaviors, the catalytic activity of pure Ag and Ag₃Sn catalysts was investigated using CVs in 1 M NaOH and 1 M NaOH +5mM NaBH₄ solution, with results shown in Figure 5a and b. It can be seen that pure Ag and Ag₃Sn catalysts almost have no catalytic current in pure NaOH solution, after adding NaBH₄, one strong oxidation current peak located at 0.864 V on pure Ag and 0.800 V on Ag₃Sn, which could be ascribed to the BOR. Further, the NaBH₄ oxidation potential was more negative on Ag₃Sn surface than that of pure Ag surface, and the NaBH₄ oxidation current density on Ag₃Sn at any potential was higher than the corresponding value of pure Ag, demonstrating that the Ag₃Sn possessed a better BOR catalytic activity than pure Ag. The negative shift of oxidation potential could be attributed to the existence of Sn atoms that enhances the electrocatalytic oxidation kinetics of NaBH₄.

To assess the stability of the catalysts during BOR process, the chronoamperometric (i-t) test in 5 mM NaBH₄ + 1 M NaOH solution was performed. As seen in Figure 5c, pure Ag exhibits a decrease in current density with time throughout the 300s test period. As for the Ag₃Sn and commercial Pt/C catalysts, the current values decrease firstly, and then tend to be stable. Figure 5d compares the current retention evaluated in comparison with the current at 25s. The degradation of the current after operating for 300s at 0.765V was 35.7%, 52.11% and 34.56%, respectively. It was indicated that the Ag₃Sn as anodic catalysts possessed a better durability than pure Ag and Pt/C due to the stable intermetallic structure.

Figure 6 shows the BOR kinetic parameters for the Ag₃Sn, pure Ag and Pt/C catalysts, which are determined from the LSVs at various rotation speeds ranging from 200 to 1400 rpm, and the corresponding K-L plots based on LSV data are drawn at different potentials. The numbers of electrons transferred calculated from the slope for the Ag₃Sn, pure Ag, and Pt/C catalysts were 7.64, 5.18, and 8.0, respectively. The value for Ag₃Sn during the NaBH₄ oxidation is close to the theoretical value of 8, indicating better BOR performance of the Ag₃Sn catalyst than pure Ag.

DISCUSSION

As seen in Table S2, the ordered Ag₃Sn catalyst had a half-wave potential ($E_{1/2}$) of 0.772 V, comparable to Ag-Cu, Ag-Co etc. Ag-Sn nanoalloys exhibited ~12 and ~1.3 times enhancement in SA with respect to pure Ag and Pt/C. After 2000 cycles, the $E_{1/2}$ of the Ag₃Sn catalyst shifted negatively about 11 mV, which was much lower than Pt/C (29 mV), indicating the superior durability of the ordered Ag₃Sn catalyst. As listed in Table S3, in spite of the very low NaBH₄ concentration, the ordered Ag₃Sn catalyst delivered a BOR current density of about 11.332 mA cm⁻² at 0.835V, better than most of the Ag-based alloys.

The XPS survey spectra of the Ag₃Sn, pure Ag and pure Sn catalysts are shown in Figure 7a and S11a. The peaks of Ag and Sn are clear in the Ag₃Sn catalyst, with Ag/Sn in a 2.92 at% ratio. Figure 7b and S11b display the high-resolution spectra of Ag 3d core levels. The binding energy of the Ag 3d_{3/2} orbital was 374.27 eV for both pure Ag and Ag₃Sn, which matched metallic silver (Ag⁰). It is surprising to find that the peak of binding energy of the Ag 3d_{3/2} orbital for the Ag₃Sn catalyst had no shift compared with that of pure Ag. Figure 7c and S11c display the deconvoluted XPS spectra of Sn 3d. The binding energies of Sn 3d_{3/2} and 3d_{5/2} orbitals were 493.25 and 484.87 eV, which were ascribed to metallic tin (Sn⁰). The two peaks at 494.64 and 486.24 eV were attributable to Sn 3d peaks of Sn oxide (Sn^{x+}), consistent with the reported article⁴⁴. Figure 7d shows the XPS spectrum of O 1s. The binding energy peak centered at 530.1 eV, resulting from O²⁻ at the intrinsic sites⁴⁵. The binding energies and surface composition of several different catalysts obtained by XPS analysis are summarized in Table S4.

Figure 8a and S11d show the valence band spectrum (VBS) of Ag₃Sn, pure Ag, and pure Sn catalysts. The d-band center positions of pure Sn, pure Ag, and Ag₃Sn catalysts were 3.83, 5.34 and 5.40 eV, respectively. It is unexpected to find that the d-band center of the Ag₃Sn catalyst (5.40 eV) was more far away or downshifting from the Fermi energy level than that of pure Ag (5.34 eV), as the upshift of the d-band center results in higher adsorption strength with oxygen, thereby improving ORR catalytic activity for Ag-based nanoalloys²⁷. As shown in Figure 8b, the electron densities of states of these catalysts are also calculated by the DFT method to examine the d-band center, and the calculated values coincide with the experimental VBS. According to the DFT calculations results, the d-band center of Ag₃Sn (111) shifts down by 0.27 eV in comparison with Ag (111), which reduces the bonding with O and OH and thereby accelerates

the removal of O and OH. However, the Sn atoms have stronger affinity to oxygen, which benefits the initial oxygen binding.⁴⁶

These obtained outcomes demonstrate a unique ability of the Ag₃Sn catalyst to catalyze the four-electron reduction to yield OH⁻. Moreover, Ag is only active for the two-electron pathway in basic solution, due to its weak affinity to oxygen (seen in Figure 8c). Many researchers have pointed out electronic interaction as the probable origin for the enhanced electrocatalytic four-electron ORR. For example, Baker⁴⁶, Gatewood⁴⁷ and Miah⁴⁸ proposed a bifunctional mechanism to explain the enhanced catalytic activity of Au-SnO_x or AuSn catalysts, in which O₂ is chemisorbed onto the Sn or SnO_x surface in the form of O₂⁻, and then further reduced on Au. Lu³¹ has also referred a similar enhanced catalytic activity of Ag₄Sn/C to a bifunctional mechanism.

In this work, the improved catalytic activity may be related to the surface species of the Ag₃Sn catalyst, which contains Ag, Sn, SnO_x. As shown in schematic illustration of Figure 8d, the main origin of the enhanced catalytic performance of the Ag₃Sn catalyst can be inferred as ensemble effect. O₂ is chemisorbed onto Sn and SnO_x sites in the form of the superoxide radical (O₂^{•-})_{ads} or hydroperoxide radical (OOH[•])_{ads}. The (O₂^{•-})_{ads} then convert or spill over onto the Ag site and is further reduced on Ag sites. The resulting hydroxyl species (OH⁻) could easily leave the surface. Formation of the initial intermediate (i.e., (O₂^{•-})_{ads}) at the Ag is difficult, but once it is formed at the Sn site, it can then be easily reduced at the Ag site producing the final product.

As far as we are aware, the bimetallic nanoparticles can serve as an important and effective approach to improve the catalytic activities of Ag-based electrocatalysts, which can be cataloged into three kinds of nanostructures, that is, heterogeneous core-shell nanoparticle (i.e., Ni@Ag²²

Cu@Ag²³), homogeneous random alloy (e.g. Ag-Au⁴⁹, Ag-Pd¹⁴), and ordered intermetallic (i.e., Ag₄Sn³¹, AgPt⁵⁰). The ordered nano-intermetallic compounds are unique and stable bimetallic nanostructures with long-range order in atomic arrangement⁵⁰, are the most effective in both separating the active surface sites and adjusting the surface electronic properties⁵¹. Therefore, Ag-based intermetallic compounds alloying with the main group metal, transition metal or rare earth are recognized as a novel method to design material.^{28-30, 52-54} Unfortunately, the preparation of Ag-rich intermetallic compounds with high phase-purity is a challenging task due to the very low reduction potentials of some alloying elements (Ti⁴⁺, Sc³⁺, and lanthanide cations) even at high temperatures or using chemical agents.⁵⁵ Therefore, it is worthy that this study provides a new ensemble concept for achieving and understanding high catalytic activity in the Ag₃Sn intermetallic electrocatalysts, which are fundamentally different from those core-shell and alloy Ag-based electrocatalysts relied on the electronic effect.^{27, 56-59}

CONCLUSIONS

A novel orthorhombic Ag₃Sn intermetallic compound as bifunctional electrocatalyst for ORR and BOR has been successfully synthesized by a green electrodeposition method. The catalytic performance of as-synthesized Ag₃Sn for both ORR and BOR in alkaline media is superior to pure Ag. What's more, the excellent durability of intermetallic microstructure provides another advantage for Ag₃Sn to be a potentially bifunctional catalyst in DBFC. The enhanced ORR activity for the intermetallic Ag₃Sn may arise from the ordered structure and ensemble effect which promote the steps of oxygen reduction.

EXPERIMENTAL SECTION

Materials. Silver sulfate (Ag_2SO_4), thiourea ($\text{SC}(\text{NH}_2)_2$), Stannous sulfate (SnSO_4), Sulfuric acid (H_2SO_4), potassium hydroxide (KOH), sodium hydroxide (NaOH), Ethanol ($\text{C}_2\text{H}_5\text{OH}$) and sodium borohydride (NaBH_4) were purchased from Tianjin Fuchen Chemical Reagent Co. Ltd. The Pt/C catalyst (20 wt %) was obtained from Johnson Matthey Fuel Cells. Nitrogen (N_2) and Oxygen (O_2) (99.99%) gases were used as received from Xi'an Taida Chemical Reagent Co. Ltd.

Synthesis of the Ag_3Sn catalyst. The electrodeposition current was optimized through the voltammetric experiment, as seen in Figure S1, one cathodic peak appeared at -0.557 V due to the co-deposition of Ag and Sn. A deposition current of -10 mA cm^{-2} for 150 s was used to fabricate Ag-Sn alloy in a 2 M H_2SO_4 solution composed of 0.02M SnSO_4 and 0.01 M Ag_2SO_4 . A glassy carbon electrode (GCE, 5 mm in diameter) was employed as the working electrode for the electrochemical measurements, while the Cu foil substrate (deposition area: $\text{ca.}1\text{cm}^2$) was used as the working electrode for characterization. The platinum foil faced to the GCE, and saturated calomel electrode (SCE) was used as the reference electrode. Before using, glassy carbon electrode (GCE) was polished with 0.05-3 micron Al_2O_3 slurry, followed by rinsing with ultrapure water and ethanol. The total concentration of each precursor electrolyte was 40 mM, and thiourea was added to each precursor as a complexing agent. After electrodeposition, the modified GCE was washed carefully with ultrapure water. For comparison during the electrochemical measurement, pure Ag and pure Sn as a control were also synthesized under the same experimental conditions.

Physical characterization. The crystal structure was characterized by X-ray diffraction (XRD) with Cu $\text{K}\alpha$ radiation (PANalytical X'Pert Pro MPD), and the morphology and structure were investigated using a field-emission scanning electron microscopy (FESEM, FEI NovaSEM 450)

equipped with energy dispersive X-ray spectrometer (EDX) and transmission electron microscopy (TEM, FEI Tecnai F30). The surface components and electron structure were determined by an X-ray photoelectron spectra (XPS, ESCALAB 250) with a monochromatic Al K α X-ray source (E=1486.6 eV).

Electrochemical characterization. The electrochemical studies were carried out on a CHI 660C electrochemical workstation with a rotating disk electrode at room temperature. The platinum wire and Hg/HgO electrode (in 1 M KOH) acted as the counter electrode and reference electrode. The catalysts loading on the disk electrode was 1.3 mg cm⁻², except 0.5 mg cm⁻² for the commercial Pt/C. The potentials were reported with respect to reversible hydrogen electrode (RHE). To ensure the reproducibility of the proposed catalysts, all experimental results were repeated at least three times.

The ORR measurements were performed in O₂-saturated 0.1 M KOH electrolyte at a scan rate of 10 mV s⁻¹. While the BOR tests were measured in N₂-saturated 1M aq NaOH with 5mM NaBH₄ at a sweep rate of 10 mV s⁻¹. The cyclic voltammetric (CV) curves were examined in 0.1 M KOH or 1 M NaOH solution with N₂ saturated for comparison. The electrons transfer number (n) can be obtained according to the Koutecky-Levich eq 1, 2 and 3^{60, 61}:

$$j^{-1}=j_d^{-1}+j_k^{-1} \quad (1)$$

$$j_d= 0.62nFD^{2/3}\nu^{-1/6}C_0\omega^{1/2} \quad (2)$$

$$j_k=nFkC_0 \quad (3)$$

where j is the measured current density (mA cm⁻²) , j_k and j_d are the kinetic and diffusion limiting current density, ω is the electrode rotation speed (rad s⁻¹), n is the total number of

transferred electrons, F is the Faraday constant (96485 C mol^{-1}), D is the diffusion coefficient of O_2 in the 0.1M KOH solution ($1.9 \times 10^{-5} \text{ cm}^2 \text{ s}^{-1}$) or of BH_4^- in the 1M NaOH solution ($1.28 \times 10^{-5} \text{ cm}^2 \text{ s}^{-1}$), C_0 denotes the bulk concentration of O_2 dissolved in the electrolyte ($1.2 \times 10^{-3} \text{ mol L}^{-1}$) or the concentration of NaBH_4 ($5 \times 10^{-3} \text{ mol L}^{-1}$), ν is the kinematic viscosity of the electrolyte for the 0.1M KOH ($0.01 \text{ cm}^2 \text{ s}^{-1}$) or for 1M NaOH ($0.014 \text{ cm}^2 \text{ s}^{-1}$), and k is the electron transfer rate constant ($\text{mol cm}^3 \text{ s}^{-1}$).

The Tafel slope and the exchange current density are estimated by using the Tafel relation as⁶²:

$$\eta = a + b \log j_k \quad (4)$$

where η defines the overpotential ($\eta = E - 1.23$), j_k denotes the mass corrected kinetic current density, and b represents the Tafel slope. A more elaborate equation can be written as⁶³:

$$\eta = RT/(\alpha nF) \ln j_0 + RT/(\alpha nF) \ln j_k \quad (5)$$

where R is the ideal gas constant ($8.314 \text{ J mol}^{-1} \text{ K}^{-1}$), α is the transfer coefficient, n is the number of electrons transferred, and j_0 is the exchange current density.

Density functional theory (DFT) calculations. The spin-polarized Kohn-Sham DFT calculations were carried out with the atomic orbital-based DMol³ package code of Materials Studio⁶⁴. The Kohn-Sham equation was expanded in a double-numerical quality basis set with polarization functions (DNP)⁶⁵. We used the Perdew-Becke-Ernzerhof (PBE) flavor of DFT in the generalized gradient approximation (GGA)^{66, 67}. The range for the orbital cutoff was set to 5.0 \AA . The DFT semicore pseudopotential⁶⁸ was chosen to treat the core electrons of the heavy Ag and Sn atoms. We modeled the surface using Ag_3Sn with Ag/Sn in 75%/25% atomic ratio. Surfaces of Ag_3Sn (111) catalyst systems are modeled as a slab with a 15 \AA vacuum equivalent

to ensure periodic conditions. A (2×4) supercell-slab of the (111) surface was used to evaluate density of states.

ASSOCIATED CONTENT

The Supporting Information is available free of charge on the ACS Publications website at DOI: xxxxx.

Additional CVs, SEM, EDX, LSVs, TEM, and XPS for the catalysts (PDF).

AUTHOR INFORMATION

Corresponding Authors

*(F. C.) E-mail: fuyichen@nwpu.edu.cn.

*(R. L. J.) E-mail: r.l.johnston@bham.ac.uk.

ORCID

Fuyi Chen: 0000-0002-2191-0930

Liang An: 0000-0002-8742-576X

Roy L. Johnston: 0000-0003-4019-9280

Notes

The authors declare no competing financial interest.

ACKNOWLEDGMENTS

This work was supported by the National Natural Science Foundation of China (grant nos. 51271148 and 50971100), the Research Fund of State Key Laboratory of Solidification Processing in China (grant no. 150-ZH-2016), the Aeronautic Science Foundation Program of China (grant no. 2012ZF53073), the Science and Technology Innovation Fund of Western Metal Materials (grant no. XBCL-2-11) and the Doctoral Fund of Ministry of Education of China (grant no. 20136102110013).

REFERENCES

- (1) Ferrando R.; Jellinek J.; Johnston R. L. Nanoalloys: From Theory to Applications of Alloy Clusters and Nanoparticles. *Chem. Rev.* **2008**, 108, 845-910.
- (2) Olu P. Y.; Job N.; Chatenet M. Evaluation of Anode (Electro)catalytic Materials for the Direct Borohydride Fuel Cell: Methods and Benchmarks. *J. Power Sources* **2016**, 327, 235-257.
- (3) Song C. Y.; Zhang D. M.; Wang B.; Cai Z.; Yan P.; Sun Y.; Ye K.; Cao D. X.; Cheng K.; Wang G. L. Uniformly Grown PtCo-Modified Co_3O_4 Nanosheets as a Highly Efficient Catalyst for Sodium Borohydride Electrooxidation. *Nano Res.* **2016**, 9, 3322-3333.
- (4) Olu P. Y.; Deschamps F.; Caldarella G.; Chatenet M.; Jobet N. Investigation of Platinum and Palladium as Potential Anodic Catalysts for Direct Borohydride and Ammonia Borane Fuel Cells. *J. Power Sources* **2015**, 297, 492-503.
- (5) Liu Y.; Li D. G.; Stamenkovic V. R.; Soled S.; Henao J. D.; Sun S. H. Synthesis of Pt_3Sn Alloy Nanoparticles and Their Catalysis for Electro-Oxidation of CO and Methanol. *ACS Catal.* **2011**, 1, 1719-1723.
- (6) Du Y.; Xu J. J.; Chen H. Y. Ultrathin Platinum Film Covered High-Surface-Area Nanoporous Gold for Methanol Electro-Oxidation. *Electrochem. Commun.* **2009**, 11, 1717-1720.
- (7) Liang Y. Q.; Cui Z. D.; Zhu S. L.; Liu Y.; Yang X. J. Silver Nanoparticles Supported on TiO_2 Nanotubes as Active Catalysts for Ethanol Oxidation. *J. Catalysis* **2011**, 278, 276-287.
- (8) Fu S. F.; Zhu C. Z.; Du D.; Lin Y. H. Facile One-Step Synthesis of Three-Dimensional Pd-Ag Bimetallic Alloy Networks and Their Electrocatalytic Activity toward Ethanol Oxidation. *ACS Appl. Mater. Interfaces* **2015**, 7, 13842-13848.

- (9) Peng Z. M.; Yang H. PtAu Bimetallic Heteronanostructures Made by Post-Synthesis Modification of Pt-on-Au Nanoparticles. *Nano Res.* **2009**, 2, 406-415.
- (10) Song X. J.; Zhang D. M. Bimetallic Ag-Ni/C Particles as Cathode Catalyst in AFCs (Alkaline Fuel Cells). *Energy* **2014**, 70, 223-230.
- (11) Yi L. H.; Wei W.; Zhao C. X.; Yang C. G.; Tian L.; Liu J.; Wang X. Y. Electrochemical Oxidation of Sodium Borohydride on Carbon Supported Pt-Zn Nanoparticle Bimetallic Catalyst and Its Implications to Direct Borohydride-Hydrogen Peroxide Fuel Cell. *Electrochim. Acta* **2015**, 158, 209-218.
- (12) Duan D. H.; Liang J. W.; Liu H. H.; You X.; Wei H. K.; Wei G. Q.; Liu S. B. The Effective Carbon Supported Core-Shell Structure of Ni@Au Catalysts for Electro-Oxidation of Borohydride. *Int. J. Hydrogen Energy* **2015**, 40, 488-500.
- (13) Duan D. H.; You X.; Liang J. W.; Liu S. B.; Wang Y. F. Carbon Supported Cu-Pd Nanoparticles as Anode Catalyst for Direct Borohydride-Hydrogen Peroxide Fuel Cells. *Electrochim. Acta* **2015**, 176, 1126-1135.
- (14) Slanac D. A.; Hardin W. G.; Johnston K. P.; Stevenson K. J. Atomic Ensemble and Electronic Effects in Ag-Rich AgPd Nanoalloy Catalysts for Oxygen Reduction in Alkaline Media. *J. Am. Chem. Soc.* **2012**, 134, 9812-9819.
- (15) Feng R. X.; Dong H.; Wang Y. D.; Ai X. P.; Cao Y. L.; Yang H. X. A Simple and High Efficient Direct Borohydride Fuel Cell with MnO₂-Catalyzed Cathode. *Electrochem. Commun.* **2005**, 7, 449-452.

- (16) Šljukić B.; Milikić J.; Santos D. M. F.; Sequeira C. A. C. Carbon-Supported Pt_{0.75}M_{0.25} (M = Ni or Co) Electrocatalysts for Borohydride Oxidation. *Electrochim. Acta* **2013**, 107, 577-583.
- (17) Finkelstein D. A.; Mota N. D.; Cohen J. L. Rotating Disk Electrode (RDE) Investigation of BH₄⁻ and BH₃OH⁻ Electro-Oxidation at Pt and Au: Implications for BH₄⁻ Fuel Cells. *J. Phys. Chem. C*, 2009, **113**, 19700-19712.
- (18) Olu P. Y.; Barros C. R.; Job N.; Chatenet M. Electrooxidation of NaBH₄ in Alkaline Medium on Well-Defined Pt Nanoparticles Deposited onto Flat Glassy Carbon Substrate: Evaluation of the Effects of Pt Nanoparticle Size, Inter-Particle Distance, and Loading. *Electrocatalysis* **2014**, 5, 288-300.
- (19) Miller H. A.; Bevilacqua M.; Filippi J.; Lavacchi A.; Marchionni A. Nanostructured Fe-Ag Electrocatalysts for the Oxygen Reduction Reaction in Alkaline Media. *J. Mater. Chem. A* **2013**, 1, 13337-13347.
- (20) Bu L. Z.; Zhang N.; Guo S. J.; Zhang X.; Li J.; Yao J. L. Biaxially Strained PtPb/Pt Core/Shell Nanoplate Boosts Oxygen Reduction Catalysis. *Science* **2016**, 354, 1410-1414.
- (21) Concha B. M.; Chatenet M. Direct oxidation of Sodium Borohydride on Pt, Ag and Alloyed Pt-Ag Electrodes in Basic Media: Part II. Carbon-Supported Nanoparticles. *Electrochim. Acta* **2009**, 54, 6119-6129.
- (22) Duan D. H.; Wang Q.; Liu H. H.; You X.; Liu S. B.; Wang Y. F. Investigation of Carbon-Supported Ni@Ag Core-Shell Nanoparticles as Electrocatalyst for Electrooxidation of Sodium Borohydride. *J. Solid State Electrochem.* **2016**, 1-13.

- (23) Duan D. H.; Liu H. H.; You X.; Wei H. K.; Liu S. B. Anodic Behavior of Carbon Supported Cu@Ag Core-Shell Nanocatalysts in Direct Borohydride Fuel Cells. *J. Power Sources* **2015**, 293, 292-300.
- (24) Duan D. H.; Liu H. H.; Wang Q.; Wang Y. F.; Liu S. B. Kinetics of Sodium Borohydride Direct Oxidation on Carbon Supported Cu-Ag Bimetallic Nanocatalysts. *Electrochim. Acta* **2016**, 198, 212-219.
- (25) Holewinski A.; CarlosIdrobo J.; Linic S. High-Performance Ag-Co Alloy Catalysts for Electrochemical Oxygen Reduction. *Nature Chem.* **2014**, 6, 828-834.
- (26) Aslam U.; Linic S. Kinetic Trapping of Immiscible Metal Atoms into Bimetallic Nanoparticles through Plasmonic Visible Light-Mediated Reduction of a Bimetallic Oxide Precursor: Case Study of Ag-Pt Nanoparticle Synthesis. *Chem. Mater.* **2016**, 28, 8289-8295.
- (27) Wu X. Q.; Chen F. Y.; Jin Y. C.; Zhang N.; R. L. Johnston. Silver-Copper Nanoalloy Catalyst Layer for Bifunctional Air Electrodes in Alkaline Media. *ACS Appl. Mater. Interfaces* **2015**, 7, 17782-17791.
- (28) Lee H. K.; Shim J. P.; Shim M. J.; Kim S. W.; Lee J. S. Oxygen Reduction Behavior with Silver Alloy Catalyst in Alkaline Media. *Mater. Chem. Phys.* **1996**, 45, 238-242.
- (29) Beer S. Z.; Sandier Y. L. Oxygen Reduction at Silver and Silver-Based Alloy Electrodes. *J. Electrochem. Soc.* **1965**, 112, 1133-1136.
- (30) Raj I. A.; Vasu K. I. Electrochemical and Oxygen Reduction Behaviour of Solid Silver-Bismuth/Antimony Electrodes in KOH Solutions. *J. Appl. Electrochem.* **1993**, 23, 728-734.

- (31) Lu Y. J.; Zhang N. L.; An L.; Li X.; Xia D. G. Synthesis of High Dispersed Intermetallic Ag₄Sn/C and Its Enhanced Oxygen Reduction Reaction Activity. *J. Power Sources* **2013**, 240, 606-611.
- (32) Maroun F.; Ozanam F.; Magnussen O. M.; Behm R. J. The Role of Atomic Ensembles in the Reactivity of Bimetallic Electrocatalysts. *Science* **2001**, 293, 1811-1814.
- (33) Bocanegra S. A.; Miguel S. R. D.; Borbath I.; Margitfalvi J. L.; Scelza O. A. Behavior of Bimetallic PtSn/Al₂O₃, Catalysts Prepared by Controlled Surface Reactions in the Selective Dehydrogenation of Butane. *J. Mol. Catal. A* **2009**, 301, 52-60.
- (34) Berndt H.; Mönnich I.; Lücke B.; Menzel M. Tin Promoted Palladium Catalysts for Nitrate Removal from Drinking Water. *Appl. Catal. B* **2001**, 30, 111-122.
- (35) Yuan D. W.; Liu Z. R. Atomic Ensemble Effects on Formic Acid Oxidation on PdAu Electrode Studied by First-Principles Calculations. *J. Power Sources* **2013**, 224, 241-249.
- (36) Zhou R. F.; Shi Zhang Q. Silver/Nitrogen-Doped Graphene Interaction and Its Effect on Electrocatalytic Oxygen Reduction. *Chem. Mater.* **2014**, 26, 5868-5873.
- (37) Wang J. L.; Chen F. Y.; Jin Y. C.; R. L. Johnston. Highly Active and Stable AuNi Dendrites as an Electrocatalyst for the Oxygen Reduction Reaction in Alkaline Media. *J. Mater. Chem. A* **2016**, 4, 17828-17837.
- (38) Zeng L.; Zhao T. S.; An L. A High-Performance Supportless Silver Nanowire Catalyst for Anion Exchange Membrane Fuel Cells. *J. Mater. Chem. A* **2015**, 3, 1410-1416.

- (39) Lu Y. Z.; Chen W. Size Effect of Silver Nanoclusters on Their Catalytic Activity for Oxygen Electro-Reduction. *J. Power Sources* **2012**, 197,107-110.
- (40) Liu R. J.; Li S. W.; Yu X. L.; Zhang G. J.; Ma Y.; Yao J. N. Facile Synthesis of a Ag Nanoparticle/Polyoxometalate/Carbon Nanotube Tri-Component Hybrid and Its Activity in the Electrocatalysis of Oxygen Reduction. *J. Mater. Chem.* **2011**, 21, 14917-14924.
- (41) Lima F. H. B.; Sanches C. D.; Ticianelli E. A. Physical Characterization and Electrochemical Activity of Bimetallic Platinum-Silver Particles for Oxygen Reduction in Alkaline Electrolyte. *J. Electrochem. Soc.* **2005**, 152, A1466-A1473.
- (42) Song Y.; Liu K.; Chen S. AgAu Bimetallic Janus Nanoparticles and Their Electrocatalytic Activity for Oxygen Reduction in Alkaline Media. *Langmuir* **2012**, 28, 17143-17152.
- (43) Yang Y.; Fei H. L.; Ruan G. D.; Li L.; Wang G. K.; Kim N. D.; Tour J. M. Carbon-Free Electrocatalyst for Oxygen Reduction and Oxygen Evolution Reactions. *ACS Appl. Mater. Interfaces* **2015**, 7, 20607-20611.
- (44) Zhang H.; Zhang J. W.; Lan Q. Q.; Ma H. B.; Qu K.; Inkson B. J.; Mellors N. J.; Xue D. S.; Peng Y. Nanoscale Characterization of 1D Sn-3.5Ag Nanosolders and Their Application into Nanowelding at the Nanoscale. *Nanotechnology* **2014**, 25, 425301-425312.
- (45) Luc W.; Collins C.; Wang S. W.; Xin H. L.; He K.; Kang Y. J.; Jiao F. Ag-Sn Bimetallic Catalyst with a Core-Shell Structure for CO₂ Reduction. *J. Am. Chem. Soc.* **2017**, 139, 1885-1893.

- (46) Baker W. S.; Pietron J. J.; Teliska M. E.; Bouwman P. J.; Ramaker D. E.; Swider-Lyons K. E. Enhanced Oxygen Reduction Activity in Acid by Tin-Oxide Supported Au Nanoparticle Catalysts. *J. Electrochem. Soc.* **2006**, 153, A1702-A1707.
- (47) Gatewood D. S.; Ramaker D. E.; Sasaki K.; Swider-Lyons K. E. Support Effects on Water Activation and Oxygen Reduction over Au-SnO_x Electrocatalysts Observed with X-Ray Absorption Spectroscopy. *J. Electrochem. Soc.* **2008**, 155, B834-B842.
- (48) Miah M. R.; Ohsaka T. Electrocatalysis of Underpotential Deposited Tin-Adatoms-Modified Gold Electrodes toward Oxygen Reduction Reaction in Acidic Media. *J. Electrochem. Soc.* **2009**, 156, B429-B435.
- (49) Hu P. G.; Song Y.; Chen L. M.; Chen S. W. Electrocatalytic Activity of Alkyne-Functionalized AgAu Alloy Nanoparticles for Oxygen Reduction in Alkaline Media. *Nanoscale* **2015**, 7, 9627-9636.
- (50) Cui Z. M.; Chen H.; Zhao M. T.; DiSalvo F. J. High-Performance Pd₃Pb Intermetallic Catalyst for Electrochemical Oxygen Reduction. *Nano Lett.* **2016**, 16, 2560-1583.
- (51) Pan Y. T.; Yan Y. Q.; Shao Y. T.; Zuo J. M.; Yang H. Ag-Pt Compositional Intermetallics Made from Alloy Nanoparticles. *Nano Lett.* **2016**, 16, 6599-6603.
- (52) Cable R. E.; Schaak R. E. Low-Temperature Solution Synthesis of Nanocrystalline Binary Intermetallic Compounds Using the Polyol Process. *Chem. Mater.* **2005**, 17, 6835-6841.
- (53) Davies R. A.; Ardalan S.; Mu W. H.; Tian K.; Farsaikiya F.; Darvell B. W.; Chass G. A. Geometric, Electronic and Elastic Properties of Dental Silver Amalgam γ -(Ag₃Sn), γ_1 -(Ag₂Hg₃), γ_2 -(Sn₈Hg) Phases, Comparison of Experiment and Theory. *Intermetallics* **2010**, 18, 756-760.

- (54) McMasters O. D.; Gschneidner K. A.; Venteicher R. F. Crystallography of the Silver-Rich Rare-Earth-Silver Intermetallic Compounds. *Acta Cryst.* **1970**, B26, 1224-1229.HER
- (55) Furukawa S.; Komatsu T. Intermetallic Compounds: Promising Inorganic Materials for Well-Structured and Electronically Modified Reaction Environments for Efficient Catalysis. *ACS Cataly.* **2017**, 7, 735-765.
- (56) Zhang N.; Chen F. Y.; Wu X. Q.; Wang Q.; Qaseem A.; Xia Z. H. Activity Origin of Core-Shell and Alloy AgCu Bimetallic Nanoparticles for Oxygen Reduction Reaction. *J. Mater. Chem. A* **2017**, 5, 7043-7054.
- (57) Wu X. Q.; Chen F. Y.; Zhang N.; Lei Y. M.; Jin Y. C; Qaseem A.; Johnston R. L. Activity Trends of Binary Silver Alloy Nanocatalysts for Oxygen Reduction Reaction in Alkaline Media. *Small* **2017**, 1603387.
- (58) Wu X. Q.; Chen F. Y.; Zhang N.; Qaseem A.; Johnston R. L. Engineering Bimetallic Ag-Cu Nanoalloys for Highly Efficient Oxygen Reduction Catalysts: A Guideline for Designing Ag-based Electrocatalysts with Activity Comparable to Pt/C-20%. *Small* **2017**, 1603876.
- (59) Shin, K.; Kim, D. H.; Yeo, S. C.; Lee, H. M. Structural Stability of AgCu Bimetallic Nanoparticles and Their Application as a Catalyst: A DFT Study. *Catal. Today* **2012**, 185, 94-98.
- (60) Yang Y.; Fei H. L.; Ruan G. D.; Li L.; Wang G. K.; Kim N. D.; Tour J. M. Protein Corona Influences Cellular Uptake of Gold Nanoparticles by Phagocytic and Nonphagocytic Cells in a Size-Dependent Manner. *ACS Appl. Mater. Interfaces* **2015**, 7, 20568-20575.

- (61) Yi L. H.; Wei W.; Zhao C. X.; Tian L.; Liu J.; Wang X. Y. Enhanced Activity of Au-Fe/C Anodic Electrocatalyst for Direct Borohydride-Hydrogen Peroxide Fuel Cell. *J. Power Sources* **2015**, 285, 325-333.
- (62) Jiao Y.; Zheng Y.; Jaroniec M.; Qiao S. Z. Origin of the Electrocatalytic Oxygen Reduction Activity of Graphene-Based Catalysts: A Roadmap to Achieve the Best Performance. *J. Am. Chem. Soc.* **2014**, 136, 4394-4403.
- (63) Shinagawa T.; Garciaesparza A. T.; Takanabe K. Insight on Tafel Slopes from a Microkinetic Analysis of Aqueous Electrocatalysis for Energy Conversion. *Scientific Reports* **2015**, 5, 13801-13821.
- (64) Delley B. From Molecules to Solids with the DMol³ Approach. *J. Chem. Phys.* **2000**, 113, 7756-7764.
- (65) Delley B. Time Dependent Density Functional Theory with DMol³. *J. Phys.-Condens. Mat.* **2010**, 22, 384208-384214.
- (66) Perdew J. P.; Burke K.; Ernzerhof M. Generalized Gradient Approximation Made Simple. *Phys. Rev. Lett.* **1996**, 77, 3865-3868.
- (67) Ceperley D. M.; Alder B. J. Ground State of the Electron Gas by a Stochastic Method. *Phys. Rev. Lett.* **1980**, 45, 566-569.
- (68) Delley B. Hardness Conserving Semilocal Pseudopotentials. *Phys. Rev. B* **2002**, 66, 155125-155133.

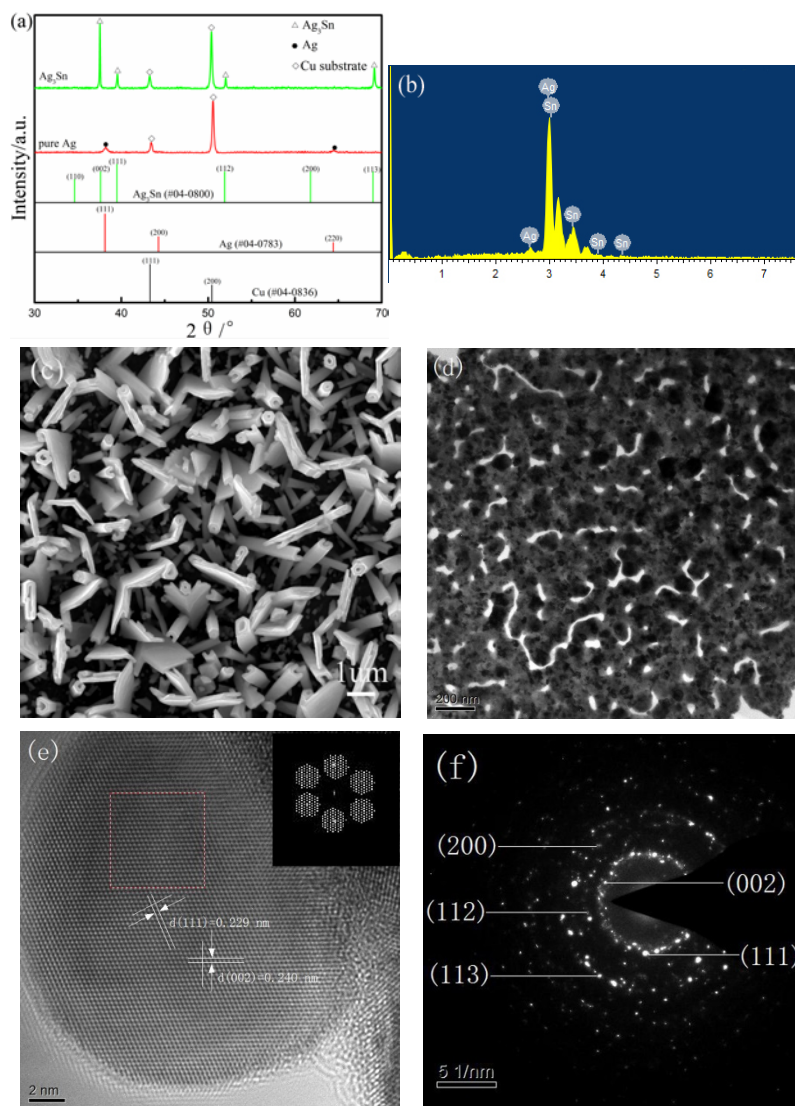


Figure 1 (a) XRD patterns of pure Ag and Ag₃Sn catalysts. (b) EDX of the Ag₃Sn catalyst. (c) SEM image of the Ag₃Sn catalyst. (d) Bright field TEM image of the Ag₃Sn catalyst. (e) HRTEM image of the Ag₃Sn catalyst and the FFT pattern corresponding to the marked square (inset). (f) SAED pattern of the Ag₃Sn catalyst.

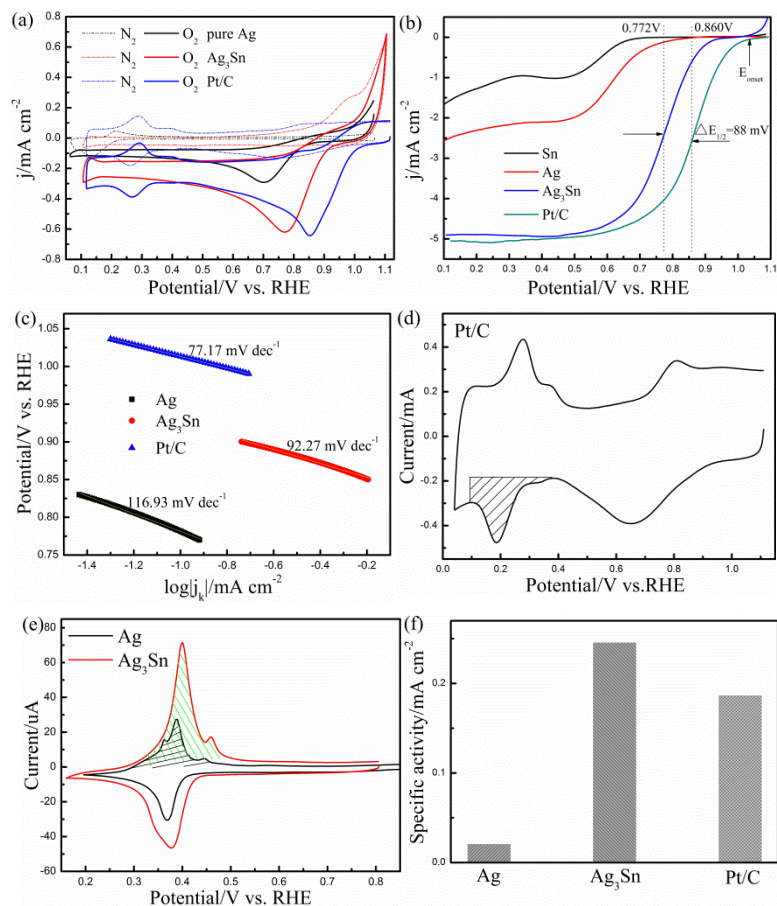


Figure 2 (a) CVs of pure Ag, Ag₃Sn and commercial Pt/C catalysts in N₂-saturated and O₂-saturated 0.1M KOH solutions at a scan rate of 10 mV s⁻¹. (b) The ORR polarization curves of the Ag₃Sn and reference (Ag, Sn, and commercial Pt/C) catalysts at a rotation rate of 1600 rpm. (c) The mass corrected Tafel plots of the Ag₃Sn, pure Ag and the commercial Pt/C catalysts. (d) CV of the commercial Pt/C recorded in N₂-saturated 0.1M KOH solution at a scan rate of 50 mV s⁻¹. (e) Pb-stripping voltammograms of the Ag₃Sn and Ag catalyst to measure the ECSA in N₂-purged electrolyte with 125 μM Pb(NO₃)₂ added after the activity measurements. (f) Specific activities of the Ag₃Sn and Ag catalysts measured at 0.8V. The specific activities were depicted as kinetic-current densities normalized to the ECSAs.

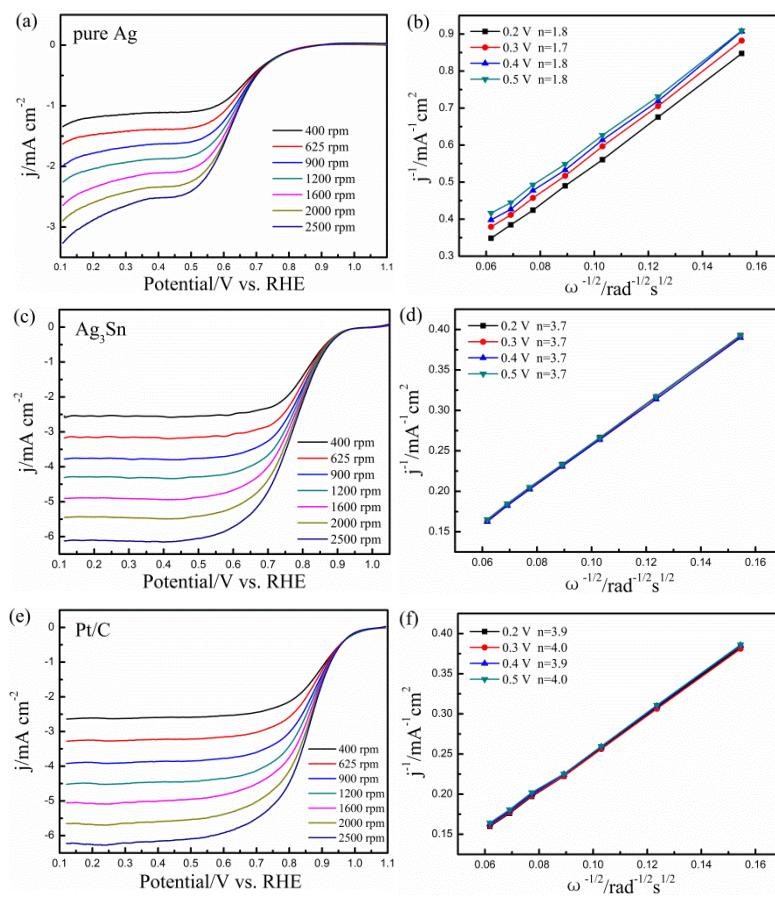


Figure 3 (a, c, e) ORR polarization curves of pure Ag, Ag₃Sn and the commercial Pt/C catalysts in O₂-saturated 0.1 M KOH at different rotating rates, scan rate: 10 mV s⁻¹. (b, d, f) Koutecky-Levich plots based on the corresponding ORR data.

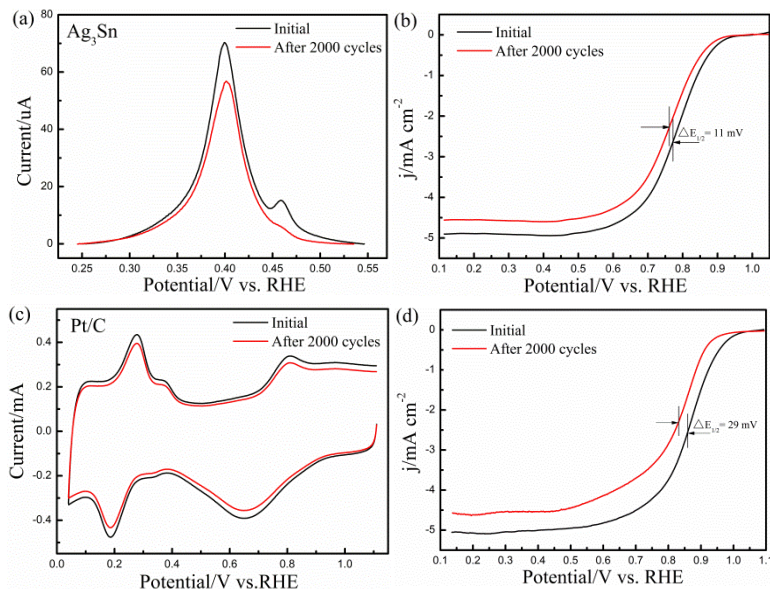


Figure 4 Comparison of ORR activities of the Ag₃Sn and commercial Pt/C catalysts before and after 2000 potential cycles. (a) Pb-stripping voltammograms of Ag₃Sn at 10 mV s⁻¹ in N₂-purged electrolyte with 125 μM Pb(NO₃)₂ (b) ORR polarization curves of Ag₃Sn catalyst in O₂-saturated 0.1 M KOH solution. (c) CVs of Pt/C in N₂-saturated 0.1 M KOH solution at 50 mV s⁻¹. (d) ORR polarization curves of Pt/C catalyst in O₂-saturated 0.1 M KOH solution.

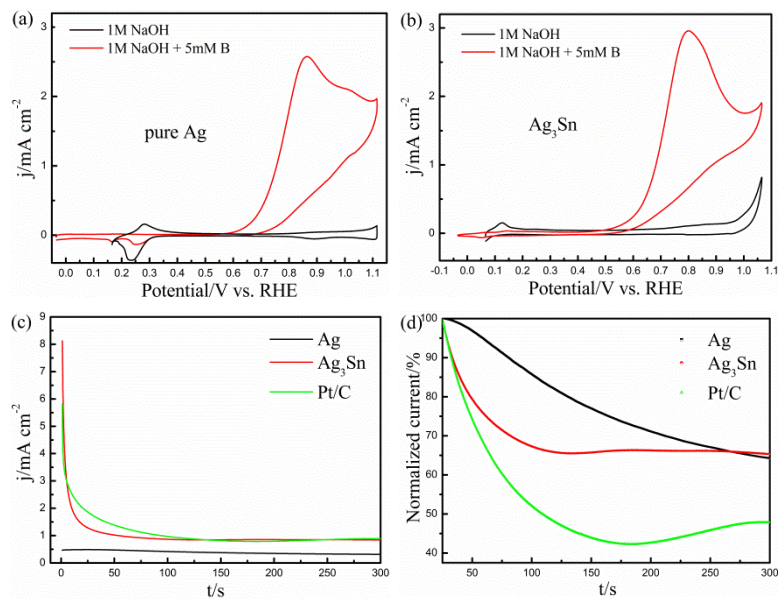


Figure 5 Cyclic voltammograms of pure Ag (a) and Ag₃Sn (b) catalysts in 1 M NaOH + 5mM (red line) and 1 M NaOH (black line) at the scan rate of 10 mV s⁻¹. Chronoamperometric curves of three different catalysts at 0.765V in 5 mM NaBH₄ + 1 M NaOH solution (c)-(d).

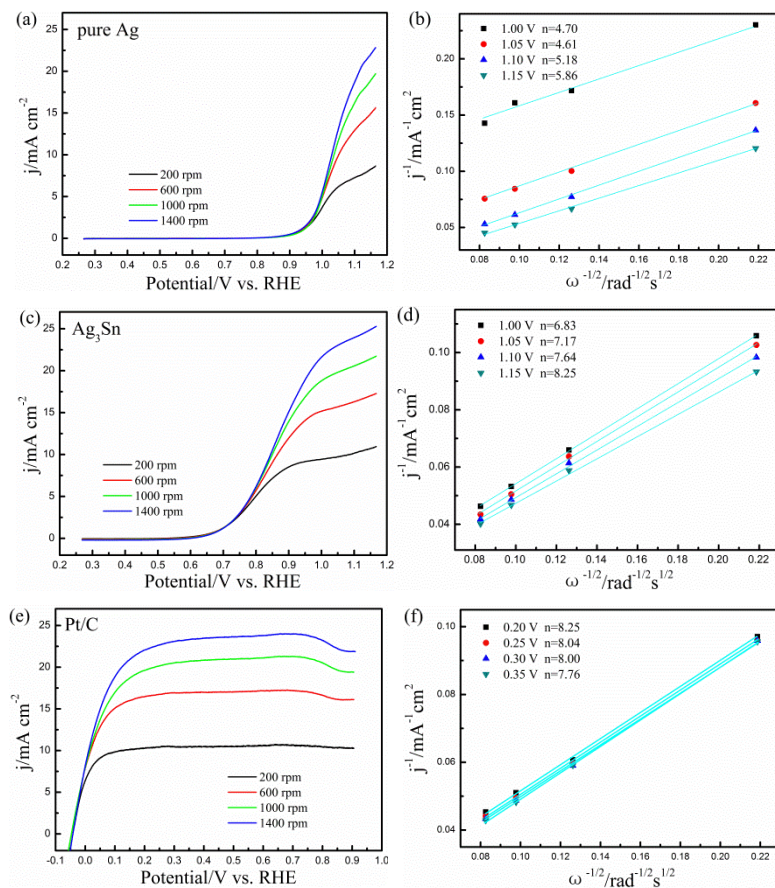


Figure 6 (a, c, e) Polarization curves of pure Ag, Ag₃Sn and the commercial Pt/C catalysts at different rotation rates in 1M NaOH solution containing 5mM NaBH₄, scan rate: 10 mV s⁻¹. (b, d, f) Koutecky-Levich plots collected from the corresponding polarization curves.

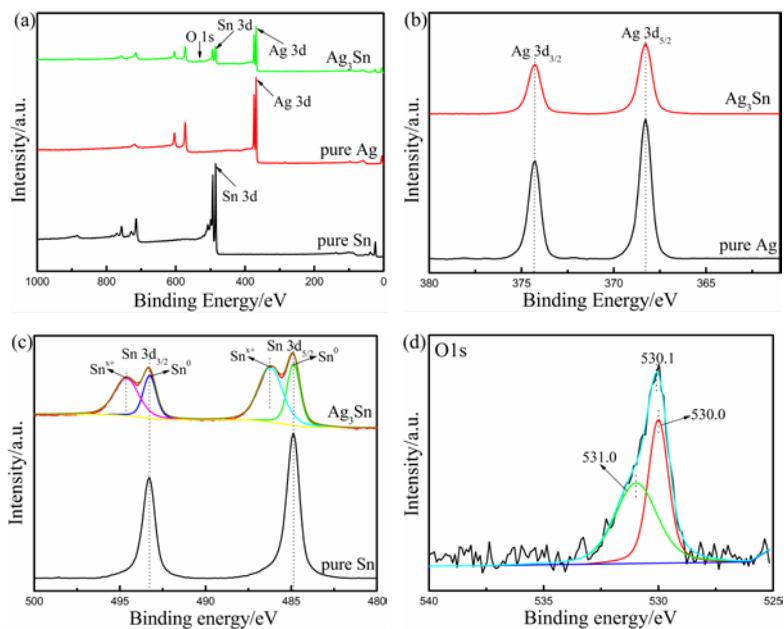


Figure 7 (a) The XPS survey spectra of Ag₃Sn, pure Ag and pure Sn catalysts. (b) High-resolution Ag 3d spectra of pure Ag and Ag₃Sn catalysts. (c) High-resolution Sn 3d spectra of pure Sn and Ag₃Sn catalysts. (d) High-resolution O 1s spectra of Ag₃Sn catalyst.

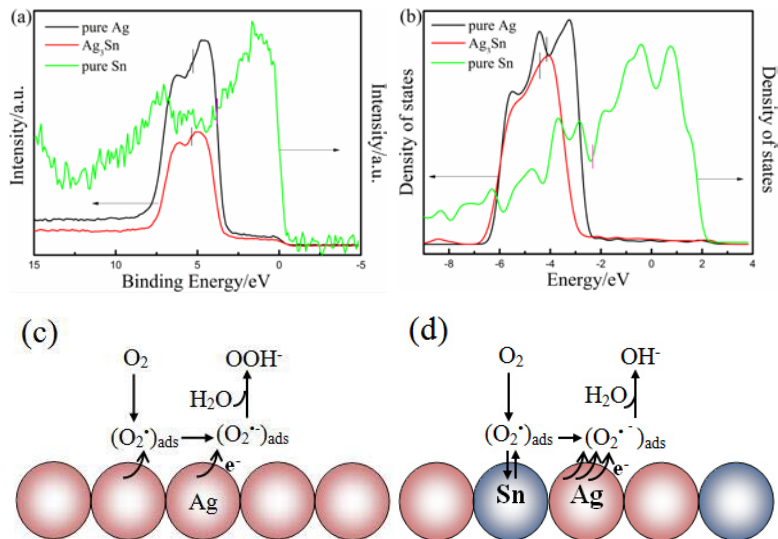


Figure 8 (a) Valence band spectrum (VBS) of Ag₃Sn, pure Ag and pure Sn catalysts. (b) Calculated valence band electron densities for Ag₃Sn, pure Ag, and pure Sn catalysts. Vertical bars represent the d-band center positions. Schematic illustrations of the adsorption and reduction of O₂ at Ag atoms (c) and the adsorption of O₂ onto Sn atoms and the reduction of the intermediate at Ag atoms (d). The arrows represent an electronic interaction.

TOC Figure

